Chapter 6
Atmosphere Attenuation and Noise Temperature at Microwave Frequencies

Shervin Shambayati

6.1 Introduction

This chapter is concerned with the effects of atmospherics on attenuation and noise temperature. These effects are universal for low-noise ground stations. Other atmospheric effects (such as those caused by the wind, which causes both defocusing and mispointing of the antenna) are much more antenna specific and are not covered here.

In general, all models and activities attempt to simplify the effects of the atmosphere into that of a homogeneous attenuator with attenuation L and physical temperature T_p. For such an attenuator, the effective noise temperature at the output of the attenuator, T_E, relates to L and T_p according to the following equation:

$$T_E = \left(1 - \frac{1}{L}\right) T_p \tag{6.1-1}$$

where L is unitless and T_p and T_E are in kelvins.

The actual atmosphere is not homogenous. Nevertheless, Eq. (6.1-1) forms the basis for calculating the atmospheric loss and the equivalent atmospheric noise temperature.

The loss L for a homogenous attenuator of length l with absorption coefficient α is given by

$$L = \exp(\alpha l) \tag{6.1-2}$$

Now consider a column of air above a station. Assuming that at any height *h* the atmospheric absorption in nepers per kilometer for frequency *f* is given by $\alpha(h, f)$; then the atmospheric loss for that frequency at height h_0 is given by:

$$L_{\text{atm}}(h_0, f) = \exp\left(\int_{h_0}^{\infty} \alpha(h, f)\, dh\right) \tag{6.1-3}$$

If the physical temperature at height *h* is given by $T_p(h)$, then for a layer of infinitesimal thickness *dh* at height *h*, the equivalent noise temperature at the bottom of the layer is given by:

$$\begin{aligned} T_E(h, f) &= \left(1 - \exp\left[-\alpha(h, f)\, dh\right]\right) T_p(h) \\ &= \left(1 - 1 + \alpha(h, f)\, dh\right) T_p(h) \\ &= \alpha(h, f)\, T_p(h)\, dh \end{aligned} \tag{6.1-4}$$

The noise temperature contribution of a layer at height *h* with infinitesimal thickness *dh* to the equivalent atmospheric noise temperature at height $h_0 < h$, $T_{\text{atm}}(h_0, f)$, is given by:

$$T_{\text{atm},h}(h_0, f) = \exp\left(-\int_{h_0}^{h} \alpha(h', f)\, dh'\right) \alpha(h, f)\, T_p(h)\, dh \tag{6.1-5}$$

Integrating Eq. (6.1-5) over *h*, yields the equation for the equivalent atmospheric noise temperature at height h_0, $T_{\text{atm}}(h_0, f)$:

$$T_{\text{atm}}(h_0, f) = \int_{h_0}^{\infty} \exp\left(-\int_{h_0}^{h} \alpha(h', f)\, dh'\right) \alpha(h, f)\, T_p(h)\, dh \tag{6.1-6}$$

If the observations take place at an angle θ, Eqs. (6.1-3) and (6.1-6) take the forms of

$$L_{\text{atm}}^{(\theta)}(h_0, f) = \exp\left(\int_{h_0}^{\infty} \frac{\alpha(h, f)}{\sin\theta}\, dh\right) \tag{6.1-7}$$

and

$$T_{\text{atm}}^{(\theta)}(h_0, f) = \int_{h_0}^{\infty} \exp\left(-\int_{h_0}^{h} \frac{\alpha(h', f)}{\sin\theta} dh' \right) \frac{\alpha(h, f)}{\sin\theta} T_p(h)\, dh \qquad (6.1\text{-}8)$$

respectively, assuming a flat-Earth model. It should be noted that due to the relative thinness of the atmosphere compared to the radius of Earth, the flat-Earth model is a very good approximation.

Note that in Eqs. (6.1-2) through (6.1-8), the absorption $\alpha(h, f)$ is expressed in nepers per unit length. In practice, $\alpha(h, f)$ is usually expressed in terms of decibels per unit length. Using decibels for the absorption $\alpha(h, f)$, Eqs. (6.1-7) and (6.1-8) could be written as

$$L_{\text{atm}}^{(\theta)}(h_0, f) = 10^{\int_{h_0}^{\infty} (\alpha(h, f)/10\sin\theta) dh} \qquad (6.1\text{-}9)$$

and

$$T_{\text{atm}}^{(\theta)}(h_0, f) = \int_{h_0}^{\infty} 10^{-\int_{h_0}^{\infty} (\alpha(h', f)/10\sin\theta) dh'} \frac{\alpha(h, f)}{4.343\sin\theta} T_p(h)\, dh \qquad (6.1\text{-}10)$$

respectively. In order to maintain consistency with the literature, through the rest of this chapter, the unit of decibels per kilometer (dB/km) is used for $\alpha(h, f)$.

In order to calculate Eqs. (6.1-9) and (6.1-10), absorption and temperature profiles $\alpha(h, f)$ and $T_p(h)$ are needed. Lacking these, direct radiometer measurements of the sky brightness temperature could be used to calculate $L_{\text{atm}}(h_0, f)$ and $T_{\text{atm}}(h_0, f)$. At the National Aeronautics and Space Administration (NASA) Deep Space Network (DSN) both direct radiometer measurements and models for $\alpha(h, f)$ and $T_p(h)$ are used to estimate $L_{\text{atm}}(h_0, f)$ and $T_{\text{atm}}(h_0, f)$. In addition, meteorological forecasts are also used to calculate $\alpha(h, f)$ and $T_p(h)$, from which $L_{\text{atm}}(h_0, f)$ and $T_{\text{atm}}(h_0, f)$ could be calculated. Section 6.2 introduces the Jet Propulsion Laboratory (JPL) standard surface model. Section 6.3 discusses the processing of the data obtained from a water vapor radiometer (WVR) and an advanced water vapor radiometer (AWVR). Section 6.4 addresses weather forecasting, and Section 6.5 provides concluding remarks.

6.2 Surface Weather Model

The surface weather model is an attempt to use ground-level meteorological measurements to calculate $\alpha(h, f)$ and $T_p(h)$ and from them obtain $L_{\text{atm}}(h_0, f)$ and $T_{\text{atm}}(h_0, f)$ for a given frequency *f*. This topic has been extensively covered in texts and papers covering remote sensing (for example, see [1]); therefore, a detailed treatment of this topic is not considered useful at this time. Hence, in this section, we only address the surface model that is used by JPL and NASA's DSN for antenna calibrations. This JPL/DSN model has been developed by Dr. Stephen D. Slobin of JPL, and it uses variations on the weather models already available for calculation of $\alpha(h, f)$ and $T_p(h)$ for the first 30 km of atmosphere above the surface height from surface meteorological measurements.

6.2.1 Calculation of $T_p(h)$

The JPL/DSN surface weather model equation for $T_p(h)$ is a variation of that for the U.S. Standard Atmosphere, 1962, model (see [1]). For the first 2 km above the surface, the temperature is calculated through a linear interpolation of the surface temperature and the temperature given by the U.S. standard atmosphere for $T_p(h)$ at a height of 2 km above the surface. Furthermore, at heights above 20 km the temperature is assumed to be a constant 217 kelvin (K). To be exact, let *h* be the height above sea level in kilometers and h_0 be the height above the sea level for the station. Then if $T_{\text{US}}(h)$ is the temperature at height according to the U.S. standard atmosphere and T_{h_0} is the measured temperature at the surface, then $T_p(h)$ is given by

$$T_p(h) = \begin{cases} T_{h_0} + \dfrac{(h-h_0)}{2}\left(T_{\text{US}}(h_0+2) - T_{h_0}\right), & h_0 \le h \le h_0 + 2 \\ T_{\text{US}}(h), & h_0 + 2 < h \le 20 \\ 217, & 20 < h \le 30 \end{cases} \qquad (6.2\text{-}1)$$

$T_{\text{US}}(h)$ for $h < 32$ km is given by [1]

$$T_{\text{US}}(h) = \begin{cases} 288.16 - 6.5h, & 288.16 - 6.5h > 217 \\ 217, & 288.16 - 6.5h \le 217,\ h < 20 \\ 197 + h, & \text{otherwise} \end{cases} \qquad (6.2\text{-}2)$$

Figure 6-1 shows a comparison of the U.S. standard model and the JPL/DSN model for $h_0 = 1$ km and $T_{h_0} = 295$ K.

6.2.2 Calculation of $\alpha(h, f)$

Radio frequency (RF) absorption characteristics of a medium are related to the resonance frequencies of that medium and how close the RF frequency is to those frequencies. In a mixture such as the atmosphere, the resonance frequencies of all molecules that comprise the medium should be taken into account. For the atmosphere, the absorption is primarily due to four factors: oxygen, water vapor, clouds (liquid water), and rain. Therefore, for a given frequency *f*, atmospheric absorption for that frequency at height *h*, $\alpha(h, f)$ could be written as:

$$\alpha(h, f) = \alpha_{\text{ox}}(h, f) + \alpha_{\text{wv}}(h, f) + \alpha_{\text{cloud}}(h, f) + \alpha_{\text{rain}}(h, f) \quad (6.2\text{-}3)$$

The oxygen contribution $\alpha_{\text{ox}}(h, f)$ depends on the oxygen content of the atmosphere at height *h*, which is a function of pressure and temperature at that height. The pressure model is based on a weighted curve-fit of the pressure profile in the U.S. standard atmosphere. This weighted curve-fit attempts to model the pressure at lower heights more accurately as this would indirectly provide us with a more accurate measure of the oxygen content of the

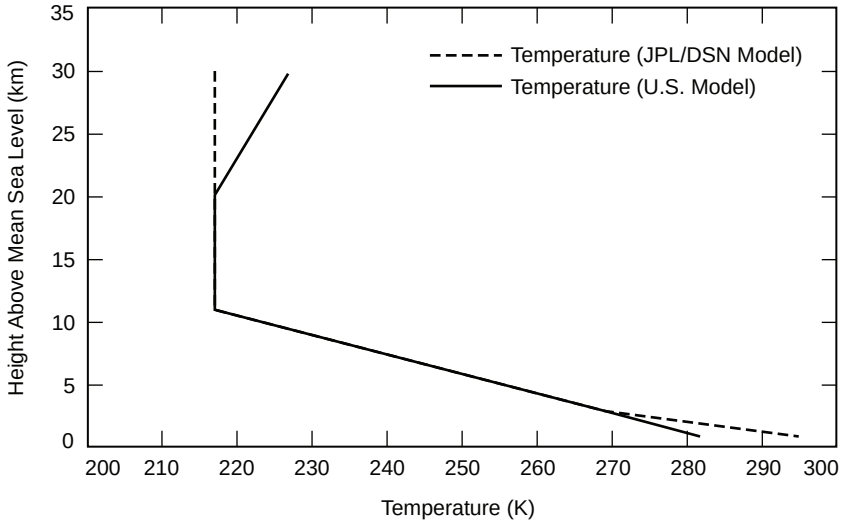

Fig. 6-1. JPL/DSN model and U.S. standard atmospheric temperature model for T_{h_0} = 295 K and h_0 = 1 km.

atmosphere. If P_{h_0} is the pressure measured at height h_0 km above the sea level, then the pressure profile for the atmosphere is calculated as:

$$P(h) = P_{h_0} \exp\left(\frac{8.387(h_0 - h)}{(8.387 - 0.0887h_0)(8.387 - 0.0887h)} \right) \qquad (6.2\text{-}4)$$

where h is height in kilometers above the mean sea level. Figure 6-2 shows a pressure profile of the atmosphere calculated from Eq. (6.2-4) for a P_{h_0} of 900 mbar at a height h_0 of 1 km.

The resonance frequencies of oxygen consist of a series of frequencies in the 50–70 GHz range (called the 60-GHz complex, see [1]) with an additional absorption line at 118.75 GHz. Due to interaction of oxygen molecules with each other and other molecules in the atmosphere, these absorption frequencies manifest themselves as two high-absorption bands around 60 GHz and 118.75 GHz. While there is a generalized model for oxygen absorption available over all frequencies, this model is very complicated. Therefore, due to the fact that as of this writing, NASA deep space missions are using only RF frequencies up to 32 GHz, the JPL/DSN surface weather model uses a simplified model that provides excellent agreement up to 45 GHz. This model is a slight modification of that presented in [1]. The absorption factor for oxygen as a function of temperature and pressure is given by

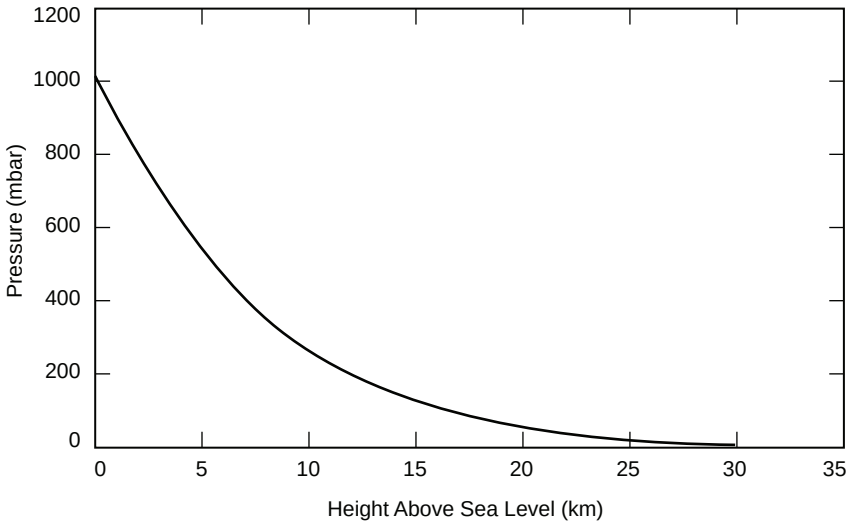

Fig. 6-2. JPL/DSN atmospheric pressure profile for P = 900 mbar (9.00×10^4 Pa) **at a height of 1 km above mean sea level.**

$$\begin{aligned}\alpha_{\text{ox}}(h,f) = \; & C(f)\gamma_0(h) f^2 \left(\frac{P(h)}{1013}\right)^2 \left(\frac{300}{T_p(h)}\right)^{2.85} \\ & \bullet \left(\frac{1}{(f-60)^2+\gamma(h)^2} + \frac{1}{f^2+\gamma(h)^2}\right) \text{dB/km}\end{aligned} \tag{6.2-5}$$

where f is frequency in gigahertz, h is the height in kilometers, $P(h)$ is the pressure in millibars at height h, and $T_p(h)$ is the temperature in kelvins at height h; $\gamma(h)$ is given by

$$\gamma(h) = \gamma_0(h)\left(\frac{P(h)}{1013}\right)\left(\frac{300}{T_p(h)}\right)^{0.85} \tag{6.2-6}$$

and $\gamma_0(h)$is given by

$$\gamma_0(h) = \begin{cases} 0.59, & P(h) > 333 \\ 0.59\left(1 + 0.0031\left(333 - P(h)\right)\right), & 25 < P(h) \le 333 \\ 1.18, & P(h) \le 25 \end{cases} \tag{6.2-7}$$

Equation (6.2-5) differs from the same equation in [1] in that the term $C(f)$ in [1] is a constant and does not depend on the frequency. However, as illustrated in [1], this constant underestimates the oxygen absorption. The JPL/DSN model uses a frequency-dependent model for $C(f)$ based on a fourth-order curve fit. Using this model, $C(f)$ is given by:

$$\begin{aligned} C(f) = \; & 0.011\left(7.13 \bullet 10^{-7} f^4 - 9.2051 \times 10^{-5} f^3\right. \\ & \left. +3.280422 \bullet 10^{-3} f^2 - 0.01906468 f + 1.110303146\right) \end{aligned} \tag{6.2-8}$$

Using Eq. (6.2-5) very good agreement is obtained with the exact model for frequencies less than 45 GHz. (see Fig. 6-3).

The water vapor attenuation and in-band radiation is dominated by two absorption bands, one at 22.2 GHz and one at 180 GHz. Again, while there is a generalized model that covers water vapor absorption for all frequencies, the DSN is only using frequencies up to 32 GHz. Therefore, the JPL/DSN model uses a simplified model applicable up to 100 GHz in the surface weather model.

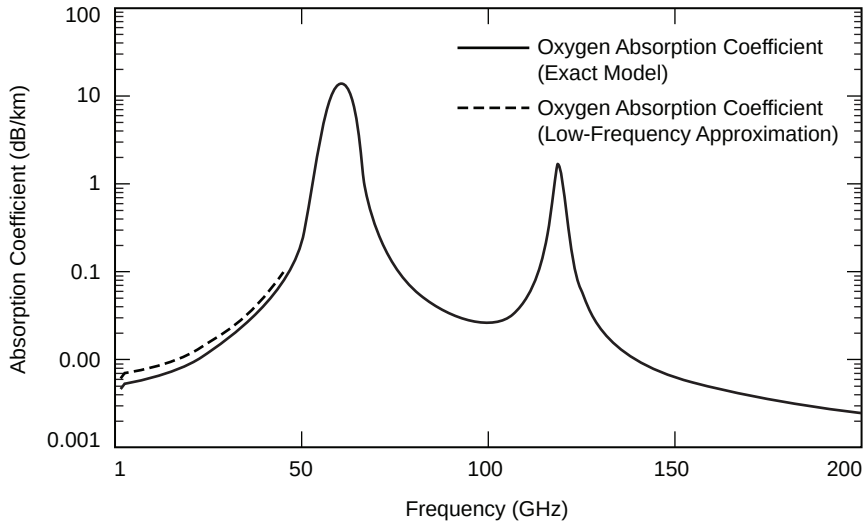

Fig. 6-3. Oxygen absorption coefficient versus frequency, T = 300 K, P = 1013 mbar (1.013×10^5 Pa)**.**

The water vapor contribution $\alpha_{\text{wv}}(h, f)$ is dependent on the absolute humidity at height *h*. Given the absolute humidity at surface $\rho_{\text{wv}}(h_0)$, the absolute humidity at height *h* is given by

$$\rho_{\text{wv}}(h) = \rho_{\text{wv}}(h_0) \exp\left(\frac{h}{H_{\text{wv}}}\right) \quad \frac{\text{g}}{\text{m}^3} \tag{6.2-9}$$

where H_{wv} is the scale height for water vapor, and it is set to 2 km. The absolute humidity at the surface, $\rho_{\text{wv}}(h_0)$, is calculated from the relative humidity at the surface r_{h_0} from the following formula:

$$\rho_{\text{wv}}(h_0) = \frac{1320.65}{T_{h_0}} r_{h_0} \bullet 10^{7.4475(T_{h_0} - 273.14)/T_{h_0} - 39.44} \quad \frac{\text{g}}{\text{m}^3} \tag{6.2-10}$$

Given $\rho(h)$, $\alpha_{\text{wv}}(h, f)$ is given by

$$\alpha_{\text{wv}}(h, f) = k_{\text{wv}}(h, f)\left(a_{\text{wv}}(h, f) + 1.2 \times 10^{-6}\right) \text{ dB/km} \tag{6.2-11}$$

where *f* is frequency in gigahertz and

$$k_{\mathrm{wv}}(h, f) = 2 f^2 \rho_{\mathrm{wv}}(h) \left(\frac{300}{T_p(h)} \right)^{1.5} \gamma_1(h) \tag{6.2-12}$$

and

$$a_{\mathrm{wv}}(h, f) = \left(\frac{300}{T_p(h) d_{\mathrm{wv}}(h, f)} \right) \exp\left(\frac{-644}{T_p(h)} \right) \tag{6.2-13}$$

and

$$d_{\mathrm{wv}}(h, f) = \left(22.2^2 - f^2 \right)^2 + 4 f^2 \gamma_1(h)^2 \tag{6.2-14}$$

and $\gamma_1(h)$ in gigahertz, the line width parameter of the water vapor, is given by

$$\gamma_1(h) = 2.85 \left(\frac{P(h)}{1013} \right) \left(\frac{300}{T_p(h)} \right)^{0.626} \left(1 + 0.018 \frac{\rho_{\mathrm{wv}}(h) T_p(h)}{P(h)} \right) \tag{6.2-15}$$

Figure 6-4 shows the $\alpha_{\mathrm{wv}}(h, f)$ for $P(h) = 1013$, $T_p(h) = 300$, and $\rho_{h_0} = 0.25$.

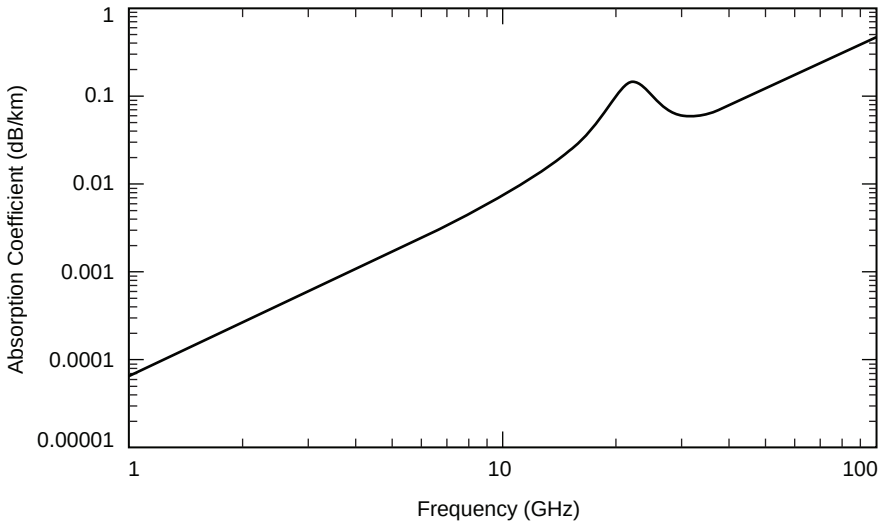

Fig. 6-4. Water vapor absorption coefficient versus frequency, T = 300 K, P = 1013 mbar (1.013×10^5 Pa)**, relative humidity = 25 percent.**

For calculating the contributions of the clouds to the atmospheric absorption, liquid water content profile of the atmosphere is needed. As this profile cannot be derived from the ground meteorological measurements, the liquid water content of the atmosphere could only be guessed at. This is the major failing of the surface weather model because, in the presence of the clouds, the surface weather model cannot give accurate modeling of the atmospheric effects. However, if the liquid water content (LWC) profile of the atmosphere $\rho_{\text{lwc}}(h)$ in grams per cubic meter (g/m^3) is known, then the cloud contribution in decibels per kilometer to $\alpha(h, f)$ is given by (see [1])

$$\alpha_{\text{cloud}}(h, f) = \rho_{\text{lwc}}(h) f^{1.95} \exp\left(1.5735 - 0.0309 T_p(h)\right) \qquad (6.2\text{-}16)$$

Figure 6-5 illustrates the $\alpha_{\text{cloud}}(h, f)$ for $\rho_{\text{lwc}}(h)$ of 0.1 g/m^3.

The rain models used in the JPL/DSN surface weather model are those developed by Olsen et al. [2]. In this model, the attenuation is calculated as a function of the rain rate. Given the rain rate in mm/h at height h, $r(h)$, the rain absorption, $\alpha_{\text{rain}}(h, f)$ is given by:

$$\alpha_{\text{rain}}(h, f) = a_{\text{rain}}(f) r(h)^{b_{\text{rain}}(f)} \qquad (6.2\text{-}17)$$

where

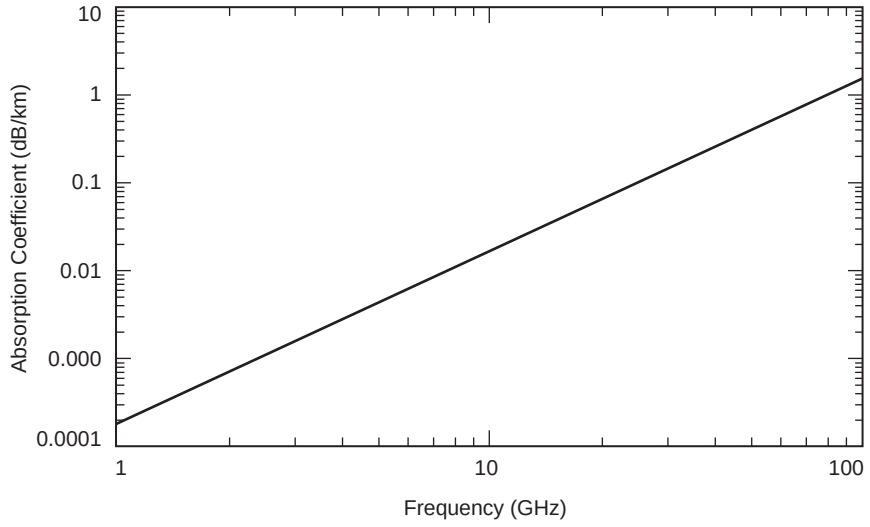

Fig. 6-5. Cloud absorption coefficient versus frequency, T = 275 K, LWC = 0.2 g/m^3**.**

$$a_{\text{rain}}(f) = \begin{cases} 6.39 \bullet 10^{-5} f^{2.03}, & f \le 2.9 \text{ GHz} \\ 4.21 \bullet 10^{-5} f^{2.42}, & 2.9 \text{ GHz} < f \le 54 \text{ GHz} \\ 4.9 \bullet 10^{-2} f^{0.699}, & 54 \text{ GHz} < f < 180 \text{ GHz} \end{cases} \quad (6.2\text{-}18)$$

and

$$b_{\text{rain}}(f) = \begin{cases} 0.851 f^{0.158}, & f \le 8.5 \text{ GHz} \\ 1.41 f^{-0.0779}, & 8.5 \text{ GHz} < f \le 25 \text{ GHz} \\ 2.65 f^{-0.272}, & 25 \text{ GHz} < f < 164 \text{ GHz} \end{cases} \quad (6.2\text{-}19)$$

Figure 6-6 shows $\alpha_{\text{rain}}(h, f)$ for r(h) = 2 mm/hr.

Again, note that in Eq. (6.2-17) the rain rate at height h, $r(h)$, needs to be known. Since the surface weather measurements cannot provide information about the rain rate at heights above the ground other than through guess work, the surface weather model provides no more than an educated guess about the effects of rain on the channel. Because of the inability of the surface weather model to deal with rain and clouds, direct radiometric measurements of the atmosphere are needed. For this purpose, JPL uses several water vapor radiometers (WVRs) [5] and advanced water vapor radiometers (AWVRs) [3,4]. In the next section, use of these instruments for characterization of atmospheric noise and atmospheric loss at different frequencies is discussed.

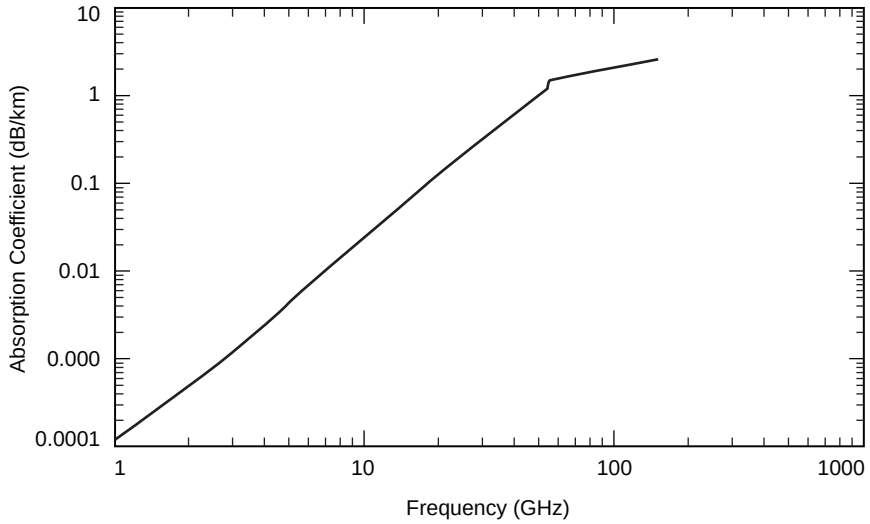

Fig. 6-6. Rain absorption coefficient versus frequency, rain rate = 2 mm/h**.**

6.3 Water Vapor Radiometer Data

6.3.1 Overview of Water Vapor Radiometer Operations and Data Processing Approach

JPL uses several types of WVRs to measure the sky brightness temperature at different elevations. The data thus recorded are processed so that the brightness temperature is referenced to zenith. Then these brightness temperature values are used to derive statistics for the zenith atmospheric noise temperature.

JPL uses several different WVRs: JT unit, D2 unit, R unit and two AWVR units. All these radiometers are Dicke radiometers. The JT unit measures the sky brightness temperatures at 20.7 GHz, 22.2 GHz, and 31.4 GHz; the D2 unit measures the sky brightness temperatures at 20.7 GHz and 31.4 GHz; and the R unit measures the sky brightness temperature at 23.8 GHz and 31.4 GHz [5]. AWVR measures the sky brightness at 22.2 GHz, 22.8 GHz, and 31.4 GHz [3]. The aggregate measurements are recorded every 3.5 minutes and checked against the radiometers health status to weed out any data that were affected by instrument malfunction. These instruments are located at the three DSN sites at Goldstone, California; Madrid, Spain; and Canberra, Australia. As of this writing (July 2005), we have 108 months of data for Goldstone, 147 months of data for Madrid, and 69 months of data for Canberra.

In standard radiometric measurements, the frequencies around 22 GHz are used to obtain the water vapor content of the atmosphere, while the 31.4-GHz frequency is used to obtain the liquid water content of the atmosphere. However, from a telecommunications point of view, we are interested in the total in-band radiation/absorption of the atmosphere. For this we use the 31.4-GHz measurements to obtain the zenith atmospheric noise temperature and then convert the zenith atmospheric noise temperature to that for the frequencies of interest (2.295 GHz [S-band], 8.42 GHz [X-band], and 32 GHz [Ka-band]).

6.3.2 Calculation of Atmospheric Noise Temperature from Sky Brightness Measurements at 31.4 GHz

Calculation of the atmospheric noise temperature, T_{atm}, from the sky brightness temperature measurements, T_B, by using the following relationship:

$$T_B = T_{\text{atm}} + \frac{T_{\text{cosmic}}}{L_{\text{atm}}} \tag{6.3-1}$$

where T_{cosmic} is the cosmic background noise temperature equal to 2.725 K, and L_{atm} is derived by substituting T_{atm} for T_E in Eq. (6.1-1), thus resulting in:

$$L_{\text{atm}} = \frac{T_p}{T_p - T_{\text{atm}}} \tag{6.3-2}$$

Substituting Eq. (6.3-2) in Eq. (6.3-1) and solving for T_{atm} results in

$$T_{\text{atm}} = T_p \left(\frac{T_B - T_{\text{cosmic}}}{T_p - T_{\text{cosmic}}} \right) \tag{6.3-3}$$

The problem with Eq. (6.3-3) is that the physical temperature of the atmosphere T_p is not known. However, practice has shown that a value of 275 K for T_p is a reasonable approximation; therefore, a physical temperature of 275 K is assumed for all calculations converting WVR and AWVR sky brightness temperature measurements to atmospheric noise temperature measurements. The AWVR and WVR data files provided for these calculations provide the sky brightness temperature measurements at zenith; therefore, the T_{atm} values that are calculated from them are also referenced to zenith.

The conversion formulas that are used to convert zenith atmospheric noise temperature values at 31.4 GHz to noise temperature values at deep space frequencies have been developed by Dr. Stephen D. Slobin of the Jet Propulsion Laboratory. The general formula for conversion of 31.4 GHz T_{atm} to 32 GHz T_{atm} is of the form

$$T_{\text{atm}}^{(32)} = T_{\text{atm}}^{(31.4)} + 5\left(1 - \exp\left(-0.008 T_{\text{atm}}^{(31.4)}\right)\right) \tag{6.3-4}$$

The conversion formulas for frequencies below 12 GHz are derived from the observation that for these frequencies the loss due to the water content of the atmosphere as well as for frequencies from 32 GHz to 45 GHz are approximately proportional to the square of the frequency (see Eqs. (6.2-11), (6.2-16), and (6.2-17)). Using this observation, we can then convert losses (in decibels) due to water vapor from 32 GHz to frequencies below 12 GHz by using a square of frequencies ratio:

$$L_{\text{H}_2\text{O}}^{(\text{dB})}(f) = L_{\text{H}_2\text{O}}^{(\text{dB})}(32)\left(\frac{f}{32}\right)^2, \qquad f < 12 \tag{6.3-5}$$

We then note that the total atmospheric loss in decibels is the sum of the losses due to water and the losses due to oxygen:

$$L_{\text{atm}}^{(\text{dB})} = L_{\text{H}_2\text{O}}^{(\text{dB})} + L_{\text{O}_2}^{(\text{dB})} \tag{6.3-6}$$

Therefore, if we know the losses due to oxygen at 32 GHz and at the frequencies of interest below 12 GHz, we can easily calculate the atmospheric losses for these frequencies from T_{atm} at 32 GHz using Eqs. (6.3-2), (6.3-5), and (6.3-6). Fortunately, the oxygen content of the atmosphere at a given site remains relatively constant and is not affected much by the weather; therefore, the surface weather model is used to calculate losses due to oxygen (see Section 6.2). These losses for deep-space S-band, X-band and Ka-band for different DSN sites are shown in Table 6-1.

Using the losses in Table 6-1 along with Eq. (6.3-2) can be used to calculate the 0-percent atmospheric noise temperature, T_{O_2}. This is the atmospheric noise temperature that would be observed if the atmosphere had no water content (vapor, liquid, or rain). These values are shown in Table 6-2.

Using values of T_{O_2} in Table 6-2, the equation for calculating the atmospheric loss for frequency $f < 12$ GHz, $L_{\text{atm}}(f)$, is given by

$$L_{\text{atm}}(f) = \left(\frac{275}{275 - T_{\text{O}_2}(f)}\right)\left(\frac{275 - T_{\text{O}_2}(32)}{275 - T_{\text{atm}}(32)}\right)^{(f/32)^2} \tag{6.3-7}$$

By using Eq. (6.3-7) in Eq. (6.1-1) we obtain the atmospheric noise temperature at frequency $f < 12$ GHz, $T_{\text{atm}}(f)$

$$T_{\text{atm}}(f) = 275\left(1 - \frac{1}{L_{\text{atm}}(f)}\right) \tag{6.3-8}$$

Table 6-1. Oxygen losses in decibels at different DSN sites for S-band (2.295 GHz), X-band (8.42 GHz), and Ka-band (32 GHz).

Site	Losses for Each Band (dB)		
	S-band	X-band	Ka-band
Goldstone	0.031	0.034	0.108
Madrid	0.032	0.036	0.114
Canberra	0.033	0.037	0.116

Table 6-2. T_{O_2} values (K) for deep space S-band, X-band, and Ka-band at different sites.

Site	0-Percent Atmospheric Noise Temperature for Each Band (K)		
	S-band	X-band	Ka-band
Goldstone	1.935	2.156	6.758
Madrid	2.038	2.273	7.122
Canberra	2.081	2.323	7.277

While Eqs. (6.3-7) and (6.3-8) are applicable to the DSN current frequencies of interest, in the future the DSN may be asked to support other frequencies. Among these are the near-Earth Ka-band (26.5 GHz), Ka-band frequencies for manned missions (37.25 GHz), and W-band (90 GHz). For these frequencies the simple frequency squared approach does not work, and different models are needed. Stephen Keihm of JPL has developed simple regression models for the sky brightness temperature. These regression models could easily be translated to regression models for the atmospheric noise temperature [6]. For W-band, the Goldstone regression formula is given by

$$T_{\text{atm}}^{(90)} = -10.81 + 4.225T_{\text{atm}}^{(31.4)} - 0.01842\left(T_{\text{atm}}^{(31.4)}\right)^2 \tag{6.3-9}$$

and for Madrid and Canberra the regression formula is given by

$$T_{\text{atm}}^{(90)} = -15.69 + 4.660T_{\text{atm}}^{(31.4)} - 0.02198\left(T_{\text{atm}}^{(31.4)}\right)^2 \tag{6.3-10}$$

For the 37.25 GHz frequency band, the regression formula for Goldstone is given by

$$T_{\text{atm}}^{(37.25)} = 1.1314 + 1.2386T_{\text{atm}}^{(31.4)} \tag{6.3-11}$$

and for Madrid and Canberra is given by

$$T_{\text{atm}}^{(37.25)} = 1.1885 + 1.241T_{\text{atm}}^{(31.4)} \tag{6.3-12}$$

Matters are slightly different for the 26.5-GHz frequency. While there is a straight linear interpolation from 31.4 GHz to 26.5 GHz, this interpolation is not very accurate due to the proximity of the 26.5 GHz frequency to the water vapor 22.2-GHz absorption band. Therefore, a formula using both the 20.7-GHz and 31.4-GHz T_{atm} values is derived. Unfortunately, not all of the radiometers measure the sky brightness in the 20.7-GHz band. Therefore,

equations both with and without 20.7-GHz T_{atm} values are presented. The equations for T_{atm} at 26.5 GHz that do not include the 20.7-GHz value of T_{atm} are

$$T_{atm}^{(26.5)} = 4.035 + 0.8147T_{atm}^{(31.4)} \tag{6.3-13}$$

for Goldstone and

$$T_{atm}^{(26.5)} = 3.4519 + 0.8597T_{atm}^{(31.4)} \tag{6.3-14}$$

for Madrid and Canberra.

The equations for T_{atm} that use the 20.7-GHz value are

$$T_{atm}^{(26.5)} = -0.11725 + 0.3847T_{atm}^{(20.7)} + 0.5727T_{atm}^{(31.4)} \tag{6.3-15}$$

for Goldstone and

$$T_{atm}^{(26.5)} = -0.09853 + 0.4121T_{atm}^{(20.7)} + 0.5521T_{atm}^{(31.4)} \tag{6.3-16}$$

for Madrid and Canberra.

6.3.3 DSN Atmospheric Noise Temperature Statistics Based On WVR Measurements

As mentioned before, the WVR data are used to generate zenith atmospheric noise temperature statistics for the DSN. These statistics are then used for link design. The cumulative statistics for S-band, X-band, and Ka-band are shown in Figs. 6-7 through 6-9 for Goldstone, Madrid, and Canberra, respectively. As seen from these figures, the zenith atmospheric noise temperature is much lower for S-band and X-band than for Ka-band. Furthermore, Ka-band frequencies have a much larger range of possible temperature values than either X-band or S-band. Also note that as the 26.5-GHz Ka-band absorption is dominated by the water vapor resonance line at 22.2 GHz, the lower percentile weather values for 26.5 GHz are actually higher than those for the 32-GHz and 31.4-GHz bands. However, for the higher percentile values, the 26.5-GHz Ka-band has lower T_z values.

Figure 6-10 shows the T_z variation observed from complex to complex for the 32-GHz Ka-band. As indicated from the T_z values, Goldstone has better weather than either Madrid or Canberra. Canberra has slightly worse weather

than Madrid. However, as the distributions shown are aggregate, this figure does not tell the whole story. At higher frequencies, seasonal variations also play a role.

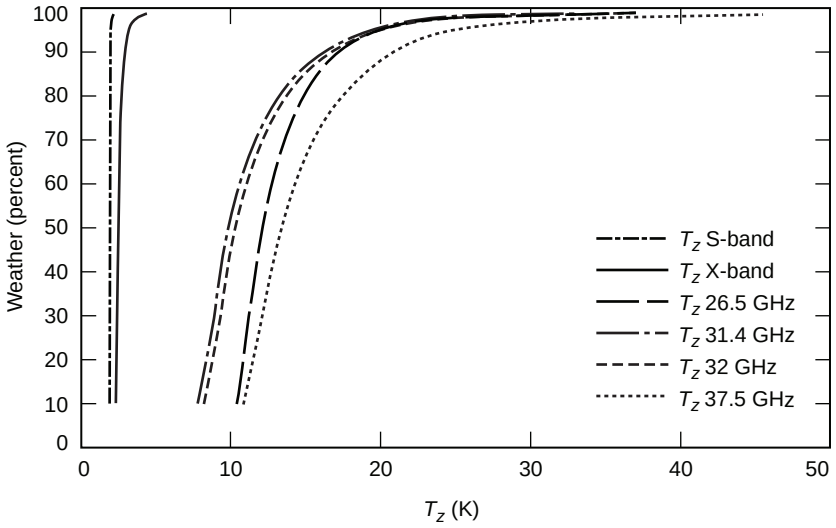

Fig. 6-7. Zenith atmospheric noise temperature (T_z) distributions for S-band, X-band, and Ka-band at the Goldstone, California, DSCC.

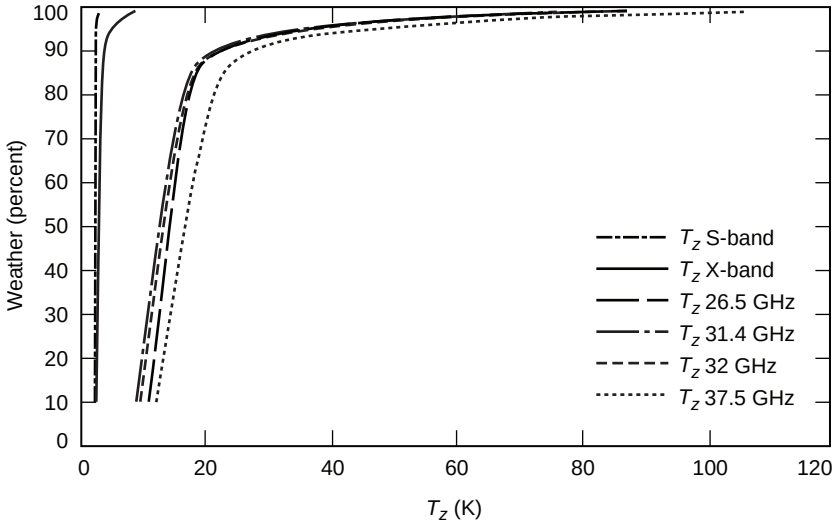

Fig. 6-8. Zenith atmospheric noise temperature distributions (T_z) for S-band, X-band, and Ka-band at the Madrid, Spain, DSCC.

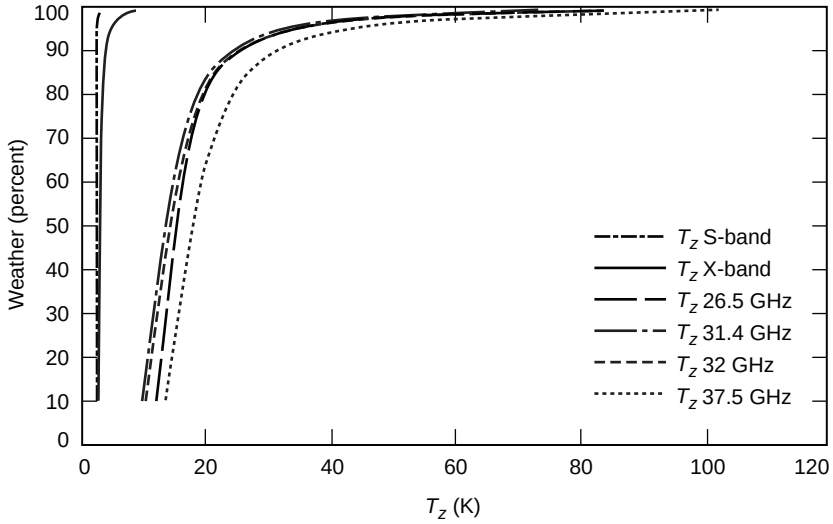

Fig. 6-9. Zenith atmospheric noise temperature distributions (T_z) for S-band, X-band, and Ka-band at the Canberra, Australia, DSCC.

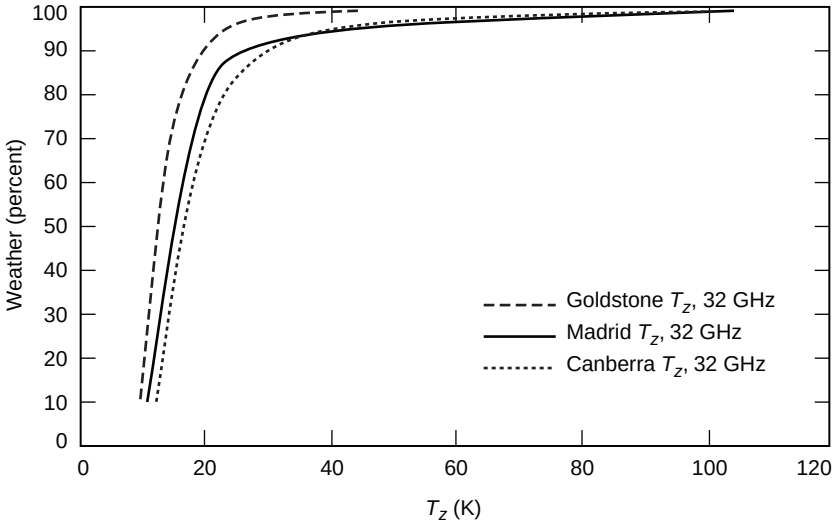

Fig. 6-10. Comparison of Goldstone, Madrid, and Canberra zenith atmospheric noise temperature distributions for the 32-GHz Ka-band.

Taking the monthly 90-percentile T_z value as an indicator of monthly T_z distributions, the weather effects could vary significantly from month to month for the higher frequencies. As seen in Fig. 6-11, Goldstone does not display much seasonal variation; however, both Madrid and Canberra have large

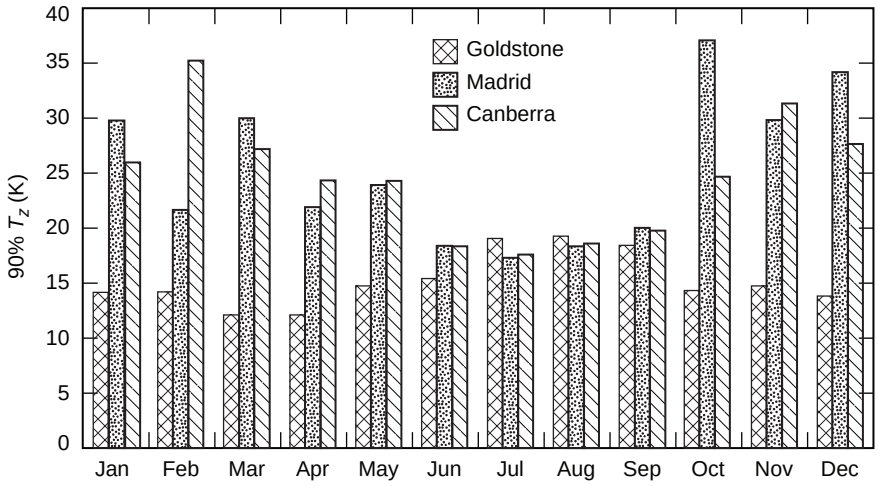

Fig. 6-11. 32-GHz Ka-band 90-percentile monthly noise temperature (T_z) values for Goldstone, Madrid, and Canberra.

weather variations during the year. For both these complexes the 90-percentile T_z for the best month is nearly half the 90-percentile T_z for the worst month.

6.4 Weather Forecasting

As seen in the previous section, weather effects at higher frequencies manifest themselves in large fluctuations in T_z. As T_z values are used in the link design, this means that for higher frequencies, the cost of reliability becomes higher in terms of margin that must be carried on the link in order to maintain a given reliability. Therefore, using just the long-term statistics means that either the link has to operated with a relatively low data rate most of the time in order achieve relatively high reliability or that the link can operate at higher data rates with lower reliability. However, if the weather effects could be predicted, then an algorithm which could adjust the data rate on the link according to weather conditions could be used in order to both maximize the link reliability and its data return capacity.

Before discussing the means of weather forecasting, one has to consider how a link is designed. The standard link equation is as follows:

$$R \bullet \left(\frac{E_b}{N_0} \right)_{(th)} = \frac{P_{SC} G_{SC}}{L_{\text{space}}} \bullet \frac{1}{L_{\text{atm}}} \bullet \frac{G_G}{kT_{\text{op}}} \qquad (6.4\text{-}1)$$

where R is the supportable data rate; $(E_b / N_0)_{(th)}$ is the required bit signal to noise ratio; P_{SC} is the spacecraft transmitted power; G_{SC} is the spacecraft antenna gain[1]; L_{space} is the space loss; L_{atm} is the atmospheric loss; G_G is the ground antenna gain; T_{op} is the system noise temperature and k is Boltzman's constant.

In Eq. (6.4-1), the term $P_{SC}G_{SC} / L_{space}$ is deterministic, depending only on the spacecraft telecommunications hardware and the distance between the spacecraft and Earth. Similarly, $(E_b / N_0)_{(th)}$ is determined by the type of channel coding that is available onboard the spacecraft, and G_G is a deterministic value. However, both L_{atm} and T_{op} are dependent on $T_z \bullet L_{atm}$, which is given by

$$L_{atm} = \frac{T_p}{T_p - T_{atm}} \tag{6.4-2}$$

where T_{atm} at elevation θ is given by

$$T_{atm} = \left(1 - \left(\frac{T_p - T_z}{T_p}\right)^{1/\sin\theta}\right) T_p \tag{6.4-3}$$

Let T_{mw} be the combined microwave noise temperature of the physical hardware that is used to track the spacecraft downlink signal. This includes the noise temperature of the antenna and the low noise amplifier (LNA). Then T_{op} is given by

$$\begin{aligned} T_{op} &= T_{mw} + T_B \\ &= T_{mw} + T_{atm} + \frac{T_{cosmic}}{L_{atm}} \end{aligned} \tag{6.4-4}$$

Given Eqs. (6.4-2) through (6.4-4), it is clear that the data rate selected in Eq. (6.4-1) is a random variable because T_z is a random variable and L_{atm} and T_{op} are functions of T_z. As in Eq. (6.4-1), a constant value for T_z must be assumed, and the selection of this value is based on the link design approach

[1] The product $P_{SC}G_{SC}$ is referred to as equivalent isotropic radiated power or EIRP.

that is taken and the distribution of T_z, $F_{T_z}(T) = \Pr\{T_z < T\}$. To put this mathematically, let $\theta(t)$ be the elevation profile of the pass for which the link is designed. Then the data rate profile for this pass, $R(t)$, is a function of $F_{T_z}(T)$ and $\theta(t)$:

$$R(t) = \gamma\left(\theta(t); F_{T_z}\right) \tag{6.4-5}$$

If T_z is relatively constant (as is the case for X-band and S-band), then the dependence of $R(t)$ on $F_{T_z}(T)$ is relatively minor. However, if like Ka-band and W-band, T_z can take a wide range of values, then dependence of $R(t)$ on $F_{T_z}(T)$ is significant as L_{atm} and T_{op} could significantly vary over time as a function of the weather, and care must be taken in selecting the proper $R(t)$ in order to take into account the uncertainty caused by variation of T_z.

In order to make the performance of the link more predictable, weather forecasting could be used to reduce the range of values that T_z could take. Let $w(t)$ be the predicted weather according to a weather forecasting algorithm. Then we can define a conditional distribution for T_z based on the weather forecast, $w(t)$:

$$F_{T_z|w(t)}(T) = \Pr\{T_z < T \mid w(t)\} \tag{6.4-6}$$

Given $F_{T_z|w(t)}(T)$, Eq. (6.4-5) is rewritten as

$$R(t) = \gamma\left(\theta(t); F_{T_z|w(t)}\right) \tag{6.4-7}$$

Note that $w(t)$ could take many forms. It could be something as simple as the date and time of the pass or as complicated as a detailed multi-layer meteorological description of the atmosphere provided by sophisticated mesonet models.

Currently, DSN is exploring the use of forecasts generated by the Spaceflight Meteorology Group at Johnson Space Flight Center for Ka-band link design. These forecasts, originally intended for use by NASA's Space Shuttle program, give a detailed multi-layer meteorological description of the atmosphere including details such as pressure, temperature, dew point, absolute

humidity, and liquid water content every 6 hours from 12 to 120 hours into the future. Therefore, each forecast set includes 19 different forecast types. (A forecast 30 hours into the future is of a different type than a forecast 36 hours into the future). Each forecast is valid for a single point in time; however, for our purposes, they could be taken as representative of the 6-hour period centered around them. The values of each forecast type were categorized, and for each category, a $F_{T_z|w(t)}(T)$ was obtained from AWVR sky brightness temperature measurements.

These forecasts were used as part of a study [7] where the values of T_z for a Ka-band link were selected according to a particular link design approach from these distributions and compared to T_z values obtained from the sky brightness temperature measurements made by the AWVR as well as with T_z values derived from monthly statistics in a "blind" test. The results are shown in Fig. 6-12. As seen from this figure, the T_z values derived from the weather forecasts follow very closely the T_z values derived from the AWVR measurements. This indicates that these forecasts could be used for adaptive link design. For a more complete treatment of this topic see [7].

6.5 Concluding Remarks/Future Directions

6.5.1 Current State

Currently most space missions use primarily X-band for their science data return; therefore, very little thought has been given to the effects of the weather on the telecommunications link performance. All but the severest weather events have very little effect on the performance of the X-band link. However, as future space missions start to use Ka-band, understanding weather effects on the link performance will become a priority.

6.5.2 Ka-Band Near-Term Development

As of this writing, several NASA and European Space Agency (ESA) spacecraft are slated to have telemetry downlink capability at Ka-band. In addition, NASA is augmenting its ground receiving capability to process both 32-GHz and 26.5-GHz Ka-band. Furthermore, ESA is building a series of 35-m beam waveguide (BWG) stations that will be Ka-band capable.

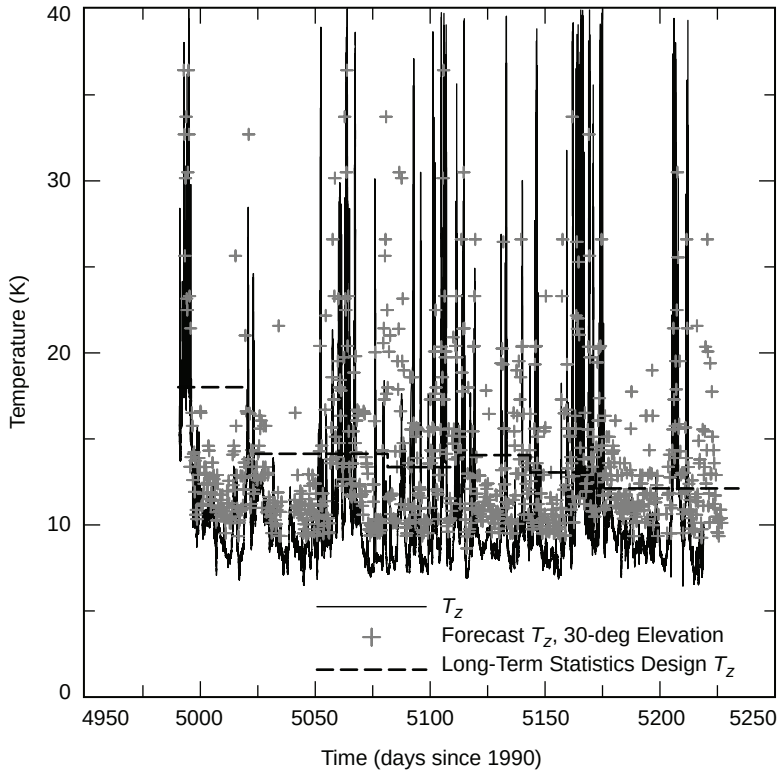

Fig. 6-12. Forecast T_z values, monthly T_z and AWVR-derived T_z measurements for Goldstone, September 2003 through April 2004.

NASA's Mars Reconnaissance Orbiter (MRO) has a fully functioning 32-GHz Ka-band downlink capability that is used for demonstration purposes. If this capability is proven reliable during the course of the demonstration, MRO will be using Ka-band to augment its science return. NASA's Kepler spacecraft and Space Interferometry Mission (SIM) spacecraft will use 32-GHz Ka-band for their primary science downlink. Lunar Reconnaissance Orbiter (LRO) and James Webb Space Telescope (JWST) will use 26.5-GHz Ka-band for their high-rate science return.

NASA has been implementing 32-GHz Ka-band support at its Deep Space Network (DSN). At this time (July 2006) the DSN has four 34-m BWG antennas capable of tracking Ka-band downlink. These are DSS 25 and DSS 26 at Goldstone Deep Space Communication Complex (DSCC) at Goldstone, California; DSS 34 at Canberra DSCC near Canberra, Australia; and DSS 55 at Madrid DSCC near Madrid, Spain. In the near future (2007–2008) plans are in place to upgrade one additional BWG antenna at Goldstone and another at Madrid to support Ka-band.

NASA is also considering implementing 37-GHz Ka-band at the DSN antennas for support of future manned missions to Mars. However, as of this writing, there are no plans in place to implement this capability.

6.5.3 Arraying

Currently, the DSN is considering replacing its monolithic 34-m and 70-m antennas with large arrays of 12-m parabolic antennas. At this time it is not clear whether or not these arrays will be located at the current DSCCs or that new complexes specifically for these antennas will be built. These antennas will be co-located and therefore, will observe the same atmospheric affects. Mathematically, let G_i be the gain of the *i*th antenna in the array and $T_{\text{op}} = T_{\text{mw}}^{(i)} + T_B$ be the system noise temperature of that antenna where $T_{\text{mw}}^{(i)}$ is the microwave noise temperature of ground equipment and T_B is sky brightness temperature observed in the line of site for the antenna. Then, assuming no combining loss, for an array of *l* antennas the signal at the receiver is

$$r = \sqrt{s}\sum_{i=1}^{l}\alpha_i\sqrt{G_i} + \sum_{i=1}^{l}\alpha_i n_i \tag{6.5-1}$$

where *s* is flux density of the signal observed at the antenna site, α_i is the optimum combining weight for the *i*th antenna (see [10]), and n_i is the noise at the *i*th antenna with a one-sided spectral density of $N_0^{(i)}$. The received signal power at the output of the combiner is $s\left(\sum_{i=1}^{l}\alpha_i\sqrt{G_i}\right)^2$. Assuming that the noise processes for different antennas in the array are independent of each other, then the signal to noise ratio at the output of the combiner is given by:

$$\frac{P}{N_0^{(\text{combined})}} = \frac{s\left(\sum_{i=1}^{l}\alpha_i\sqrt{G_i}\right)^2}{\sum_{i=1}^{l}\alpha_i^2 N_0^{(i)}} \tag{6.5-2}$$

$N_0^{(i)}$ is defined as

$$N_0^{(i)} = \mathrm{k}\left(T_{\mathrm{mw}}^{(\mathrm{i})} + T_B\right) \tag{6.5-3}$$

where k is the Boltzman constant.

Substituting Eq. (6.5-3) in Eq. (6.5-2) we obtain

$$\frac{P}{N_0^{(\mathrm{combined})}} = \frac{s\left(\sum_{i=1}^{l} \alpha_i \sqrt{G_i}\right)^2}{\sum_{i=1}^{l} \alpha_i^2 k\left(T_{\mathrm{mw}}^{(i)} + T_B\right)} \tag{6.5-4}$$

If the system noise temperature is defined by

$$T_{\mathrm{op}}^{(\mathrm{combined})} \triangleq \frac{N_0^{(\mathrm{combined})}}{\mathrm{k}} \tag{6.5-5}$$

then

$$T_{\mathrm{op}}^{(\mathrm{combined})} = \sum_{i=1}^{l} \alpha_i^2 \left(T_{\mathrm{mw}}^{(i)} + T_B\right) \tag{6.5-6}$$

Note that, as Eq. (6.5-2) indicates, the optimum combining weights, α_i, are not unique and if an l-tuple, $(\alpha_1, \alpha_2, \alpha_3, \cdots, \alpha_l)$, is a set of optimum weights, then so is $c(\alpha_1, \alpha_2, \alpha_3, \cdots, \alpha_l)$, where c is a positive constant. However, proper calculation of $T_{\mathrm{op}}^{(\mathrm{combined})}$ must be of the form

$$T_{\mathrm{op}}^{(\mathrm{combined})} = T_{\mathrm{mw}}^{(\mathrm{combined})} + T_B \tag{6.5-7}$$

Therefore, Eqs. (6.5-6) and (6.5-7) imply that

$$\sum_{i=1}^{l} \alpha_i^2 = 1 \tag{6.5-8}$$

and

$$T_{\mathrm{mw}}^{(\mathrm{combined})} = \sum_{i=1}^{l} \alpha_i^2 T_{\mathrm{mw}}^{(i)} \tag{6.5-9}$$

6.5.4 Optical

NASA is considering using optical frequencies for transmission of high-rate science data from its deep space probes in the future. A detailed description of the weather effects on the optical channel is beyond the scope of this document since these effects are substantially different than those on the RF link. These differences arise from the fact that optical channels operate at the quantum level; therefore, standard analog equations used for the RF channel do not apply. For a better treatment of this topic the reader is referred to [8,9].

6.5.5 Space-Based Repeaters

Since the weather effects become more severe at higher RF frequencies, one option that has been seriously considered is that of space-based repeaters for deep space missions. However, technological challenges and cost issues presented by such repeaters usually result in preference for ground-based antennas for tracking of deep-space missions.

Most of the technological challenges arise from the fact that the capacity of a multi-hop link (such as the one formed through the use of a repeater) is limited to that of its minimum-capacity hop. Since most space-based repeaters under consideration are Earth-orbiting, the minimum capacity hop is usually the probe-to-repeater link. Therefore, in order for a repeater-based link to compete with an Earth-based system, the capacity of the probe-to-repeater hop must be at least equal the capacity of the direct probe-to-Earth link.

For any RF receiving system, the capacity of the link is proportional to the gain-to temperature ratio (G/T). At Ka-band, for example, the G/T of a 34-m BWG for 90-percent weather at 30-deg elevation is around 60 dB with an antenna gain of about 78 dB and a system noise temperature of about 70 K. For a space-based repeater, the system noise temperature (SNT) is usually around 300 K to 450 K due to lack of cryogenically cooled LNAs. Therefore, the repeater already has a 6-dB disadvantage over the ground-based system because of the SNT. To compensate for this 6 dB, either innovative reliable space-based cryogenic technologies must be developed to reduce the receiver noise temperature on the repeater, or the gain of the antenna on the repeater must be increased.

Assuming that space-based antennas could be made as efficient as the 34-m BWG antenna regardless of size, a 68-m antenna is required to provide the 84-dB gain needed on the repeater. Needless to say, station-keeping and pointing for such a large antenna in Earth orbit requires sophisticated and advanced technologies, which are quite costly.

In addition to all these challenges, there also is the question of maintenance of such a space-based repeater network. Because these repeaters are in space, if these repeaters fail, their repair would be extremely difficult and expensive. Therefore, unless they are made reliable, space-based repeaters are of limited value.

References

[1] F. T. Ulaby, R. K. Moore, and A. K. Fung, *Microwave Remote Sensing: Active and Passive, Vol. I: Microwave Remote Sensing Fundamentals and Radiometry*, Chapter 5, Artech House, Norwood Massachusetts, pp. 256–343, 1981.

[2] R. L. Olsen, D. V. Rogers, and D. B. Hodge, "The aR^b Relation in the Calculation of Rain Attenuation," *IEEE Transactions on Antennas and Propagation*, vol. AP-26, no. 2, pp. 318–329, March 1978.

[3] A. Tanner and A. Riley, "Design and Performance of a High Stability Water Vapor Radiometer," *Radio Science*, vol. 38, no. 3, pp.15.1–15.12, March 2003.

[4] A. Tanner, "Development of a High Stability Water Vapor Radiometer," *Radio Science*, vol. 33, no. 2, pp. 449–462, March–April 1998.

[5] S. J. Keihm, "Final Report, Water Vapor radiometer Intercomparison Experiment: Platteville, Colorado, March 1–13, 1991," JPL D-8898 (JPL internal document), Jet Propulsion Laboratory, Pasadena, California, July 1991.

[6] S. Shambayati, "On the Use of W-Band for Deep-Space Communications," *The Interplanetary Network Progress Report 42-154, April–June 2003*, Jet Propulsion Laboratory, Pasadena, California, pp. 1–28, August 15, 2003.
http://ipnpr.jpl.nasa.gov/progress_report/

[7] S. Shambayati, "Weather Related Continuity and Completeness on Deep Space Ka-band Links: Statistics and Forecasting," *IEEE Aerospace Conference*, Big Sky Montana, March 5–10, 2006.

[8] R. M. Gagliardi and S. Karp, *Optical Communications*, 2nd ed., John Wiley and Sons, New York, New York, 1995.

[9] H. Hemmati, ed., *Deep Space Optical Communications*, John Wiley and Sons, New York, New York, April 2006.

[10] D. H. Rogstad, A. Mileant, and T. T. Pham, *Antenna Arraying Technique in the Deep Space Network*, John Wiley and Sons, New York, New York, January 2003.